Available online at www.sciencedirect.com

ScienceDirect

Procedia Structural Integrity 42 (2022) 911–918

Structural Integrity Procedia

www.elsevier.com/locate/procedia

23 European Conference on Fracture - ECF23

Sensitivity of numerically modelled crack closure to material

Radek Kubíček[a,b,*], Tomáš Vojtek[a], Pavel Pokorný[a], Pavel Hutař[a,b]

[a]*Institute of Physics of Materials, Czech Academy of Sciences, Zizkova 22, 612 62 Brno, Czech Republic*
[b]*Department of Engineering Mechanics, Faculty of Mechanical Engineering, Brno University of Technology. Technicka 2896/2, 61669 Brno, Czech Republic*

Abstract

Crack closure is a phenomenon which slows down fatigue crack propagation and leads to higher residual life of components and to a change in the crack front curvature. Because of the significant impact on the fatigue crack growth rate, the scientific and engineering community has been trying to describe this phenomenon very precisely. One of the most frequently described closure mechanisms is plasticity-induced crack closure (PICC) which is dominant in the Paris regime.
In the presented work, a CT specimen has been modelled three-dimensionally and the PICC estimations have been done for different models of materials to investigate their sensitivity. The models were cyclically loaded by forces inducing maximal stress intensity factor of 17 $\mathrm{MPa}\sqrt{\mathrm{m}}$ at the load ratio $R = 0.1$. The crack was curved according to conducted experiments. Even though Newman's equation estimates PICC almost constant, differences were observed from finite element simulations.

Keywords: Finite element analysis, plasticity-induced crack closure, fatigue crack growth, high cycle fatigue

1. Introduction

Since Elber first came across early crack closure during unloading due to a change in a stiffness of an aluminium CCT specimen [1], this phenomenon has been deeply studied. In many mechanical components a plastic deformation remains at the fracture surfaces after fatigue crack propagation which is responsible for the premature contact

* Corresponding author. Tel.: +0-000-000-0000 ; fax: +0-000-000-0000 .
E-mail address: kubicek@ipm.cz

2452-3216
10.1016/j.prostr.2022.12.115

between crack flanks. This plasticity-induced crack closure (PICC) is not the only mechanism which may take place [2]. The presence of oxidic layers or roughness of the crack faces play a significant role in the near-threshold fatigue crack growth [3–5]. In addition, the oxide-induced crack closure can be affected by other factors like humidity or frequency [6,7].

In a lot of studies bi-dimensional models were considered and a methodology of PICC estimation was developed [8–12]. Later, these approaches were also used for three-dimensional models to describe the behaviour locally through the thickness of the body [13–16]. 2D analyses assume a straight crack front and plane strain or plane stress conditions. Therefore, the 3D analysis is necessary to account for three-dimensional effects, such as corner singularity [17–20], which gives realistic stress-strain distribution along the crack front.

In the presented work only PICC was considered and the influence of the material was investigated at the load ratio $R = 0.1$. The NASGRO manual [21] defines the crack closure parameter f that was empirically determined from the strip-yield model [22,23]. In case of the load ratio $R = 0.1$, the parameter f does not vary sufficiently with changing material properties – yield strength σ_{y}, ultimate tensile strength σ_{UTS}, Young's modulus E or Poisson's ratio ν, see chapter 2.1. This does not agree with experiments carried out on CT specimens made of railway axle steel (bainitic steel) and crankshaft steel (pearlitic steel), where large difference in crack closure was observed [24]. The crack closure parameter f for the crankshaft steel was equal to 0.5, while for the railway axle steel the crack closure was not observed for medium fatigue crack growth rates ($f \cong R$). This difference cannot be explained by the Newman's formula in NASGRO manual.

2. Methods estimating plasticity induced crack closure

There are several methods for estimating PICC besides Newman's formula in NASGRO manual. Experimentally, the crack closure determination is based on a change of stiffness. ASTM E647 standard [25] defines an opening/closing force for compliance offset 1, 2 or 4 %. Compliance curve can be obtained from a strain record in normal direction, using a strain gauge in front of the crack or at the back face of the specimen, or by monitoring a Crack Mouth Opening Displacement (CMOD), using an extensometer [26]. Another widely used method is Digital Image Correlation (DIC) which monitors displacements on the surface near the crack tip [27]. Since DIC offers information only from the surface of the component, X-ray diffraction method was developed to monitor the deformation inside the body [28].

PICC can be determined by a numerical simulation using finite element method. The model of material must feature plasticity to develop the plastic wake behind the crack tip during the crack growth which is simulated by release of the nodes at the crack front. The moment of node release varies among the researchers; some of them simulated the crack propagation at the minimum load [29,30], the others at maximum load [8,10,29,31,32] or during the loading or unloading [11,33]. The most frequently used strategy is to release the nodes at maximum load because it has better physical meaning. Due to a correct development of crack closure, a contact between the crack faces is simulated during the unloading. Other recommendations related to the mesh size, the length of plastic wake and number of loading cycles between the node releases were adopted in the presented work, see chapter 2.2. Then the crack closure can be determined by monitoring the normal displacement of the first, or the second, node behind the crack tip or by monitoring the stress state at the crack tip. Another approach is based on the change of compliance, as in experimental determination.

In the presented work PICC estimation by strip-yield model, which is implemented in software called FASTRAN, and from the displacement of the first node behind the crack tip was considered. All the following calculations and simulations were done for the compact tension specimen (CT) with the final crack length $a_{\mathrm{f}} = 15$ mm, the width $W = 50$ mm and the thickness $B = 10$ mm loaded by forces inducing constant maximum stress intensity factor $K_{\mathrm{max}} = 17\ \mathrm{MPa}\sqrt{\mathrm{m}}$ at the load ratio $R = 0.1$, see chapter 3.1.

2.1. Parameters influencing PICC estimation in strip-yield model

FASTRAN, the software based on modified strip-yield model, was developed by James C. Newman in the mid-1970's and it simulates crack growth under variable amplitude loading [22,34]. It allows us to conduct fatigue life predictions under cycle-by-cycle simulations. The crack closure parameter f for PICC was defined in NASGRO manual [21] by Newman [35] as

$$f = A_0 + A_1 R, \qquad \text{for } R < 0 \text{ and } R \geq -2, \tag{1}$$

$$f = \max(R, A_0 + A_1 R + A_2 R^2 + A_3 R^3), \qquad \text{for } R \geq 0, \tag{2}$$

where coefficients A_0, A_1, A_2 and A_3 are defined by the following formulas including the constraint parameter α and the flow stress σ_0, which is given as arithmetic mean of yield strength and ultimate strength.

$$A_0 = (0.825 - 0.34\alpha + 0.05\alpha^2)\left[\cos\left(\frac{\pi\sigma_{\max}}{2\sigma_0}\right)\right]^{\frac{1}{\alpha}} \tag{3}$$

$$A_1 = (0.415 - 0.071\alpha)\frac{\sigma_{\max}}{\sigma_0} \tag{4}$$

$$A_2 = 1 - A_0 - A_1 - A_3 \tag{5}$$

$$A_3 = 2A_0 - A_1 - 1 \tag{6}$$

Since these formulas were defined on the basis of modified strip-yield model, the FASTRAN code (version 5.75f) was used to visualize the sensitivity of closure level on fundamental material characteristics – yield strength σ_y, ultimate tensile strength σ_{UTS}, Young's modulus E and Poisson's ratio ν. The basic values for calculations were $\sigma_y = 470$ MPa, $\sigma_{UTS} = 727$ MPa, $\nu = 0.3$ and $E = 200$ GPa. Sensitivity analysis of each material parameter is presented in Fig. 1. Only negligible change of closure level f can be seen. It means that the estimation of PICC for the maximum stress intensity factor $K_{max} = 17$ MPa$\sqrt{\text{m}}$ at the load ratio $R = 0.1$ is constant, approximately 0.3.

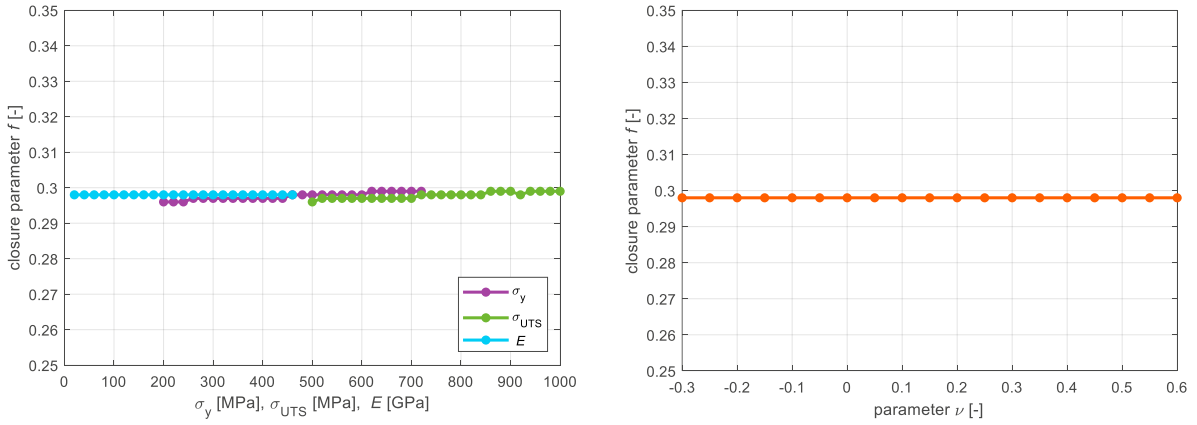

Fig. 1. Crack closure dependency on material characteristics (a) yield strength, ultimate tensile strength, Young's modulus; (b) Poisson's ratio

2.2. PICC estimation by finite element modelling

In this chapter the PICC is determined by monitoring the normal displacement of the first node behind the crack tip, u_y. Closure force F_{cl} and crack closure stress intensity factor K_{cl}, respectively, are then established by crossing the zero value of the displacement during unloading by linear interpolation, see Fig. 2. Then, the crack closure parameter f is obtained by this formula:

$$f = \frac{F_{\mathrm{cl}}}{F_{\mathrm{max}}} = \frac{K_{\mathrm{cl}}}{K_{\mathrm{max}}}. \tag{7}$$

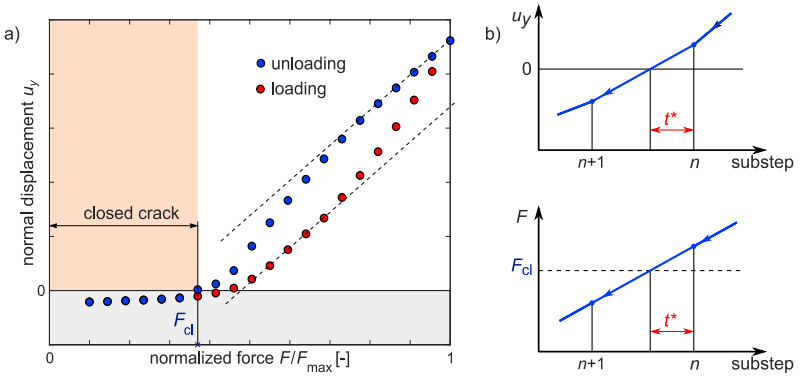

Fig. 2. Illustration of closure force determination – (a) normal displacement during loading and unloading; (b) linear interpolation.

A necessary condition to determine correct closure levels is a development of the plastic wake behind the crack tip. It is usually recommended that the total crack growth length during the simulation should be at least one size of the forward plastic zone r_{p} in order to stabilise the closure results [32,36,37]. However, it may also depend on specimen geometry, plane strain/plane stress condition, model of material or crack growth increment [15,38]. Another crucial parameter is the element length L_{e} which is equal to the crack growth increment Δa. In this study, a simple criterion defining the element length as one tenth of the forward plastic zone [32], which is defined by Irwin's second order plastic zone estimation was used:

$$r_p = \frac{1}{\alpha\pi}\left(\frac{K_{\mathrm{max}}}{\sigma_{\mathrm{y}}}\right)^2, \tag{8}$$

where α is equal to 3. Another recommendation was given by Camas [13] who defined a minimum element size at the crack tip of about $r_{\mathrm{p}}/33$ under plane stress condition. To reduce amplitude of the saw tooth residual stress pattern along the plastic wake the height of the element at the crack tip was set to be equal to L_{e} [12].

The first numerical simulations were composed only of the "growing cycles" LDU (load-debond-unload), but later the studies suggested using at least another LU cycle before each LDU. Lately, other extra LU cycles were used at the end of the procedure to stabilize the results. In the presented work, twenty growth steps were simulated in the LDU strategy with three preceding load-unload cycles. After this procedure 15 load-unload cycles were added to simulate a saturated state during fatigue loading. These twenty blocks represent the formation of the plastic wake behind the crack tip whose length was a double of the plastic zone r_{p}.

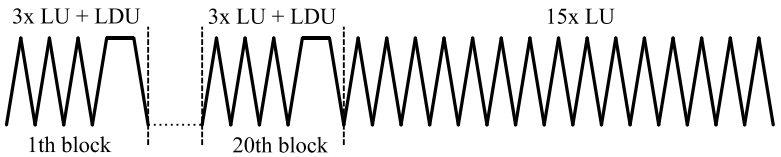

Fig. 3. Loading procedure.

3. Numerical model and materials

3.1. Geometry model

The CT specimen was loaded by forces inducing a constant maximum stress intensity factor $K_{\max} = 17$ MPa$\sqrt{\text{m}}$ at the load ratio $R = 0.1$. Since the given geometry allows using a couple of symmetries, only one-fourth of CT was modeled, see Fig. 4. The final crack length $a_f = 15$ mm, the width $W = 50$ mm and the thickness $B = 10$ mm were considered. The initial crack length a_0 was set to $a_0 = a_f - N \cdot L_e$, where $N = 20$ was the number of total cycles defining sufficient plastic wake formation.

3.2. Models of materials

The main goal of the presented work was to investigate closure levels for different materials, which was observed in experiments in [24]. Therefore, the stress-strain curve of the railway axle steel, labeled EA4T, as well as its modifications were used, see Fig. 5. These artificial curves were made by shifting up (EA4T-SU) and down (EA4T-SD) and by changing the hardening level. Greater hardening is represented by the green line (EA4T-GH), while the bilinear purple line (EA4T-BL) represents almost no hardening. All five material models were assumed to be homogenous, isotropic, elastic-plastic with kinematic hardening and Young's modulus $E = 200$ GPa and Poisson's ratio $\nu = 0.3$.

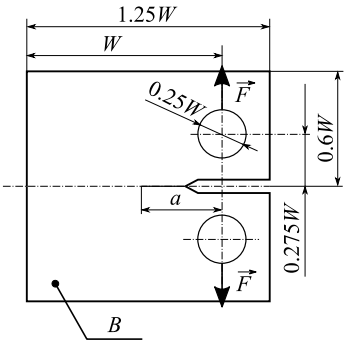

Fig. 4. Geometry model

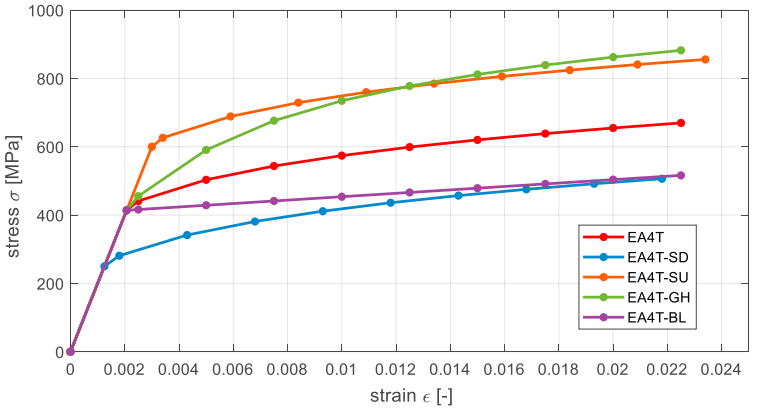

Fig. 5. Stress-strain curves of different models of materials

3.3. FE model

In the finite element model contact and linear solid elements were used. In the area around the crack tip and the developed plastic wake a homogenous and uniform structured mesh consisting of hexahedral-shaped elements, whose length L_e and height H_e were equal to one tenth of the plastic zone, was used (see Tab. 1). The crack front shape was modelled according to the conducted experiments by an exponential function $x = -0.43e^{-1.1z}$, where the parameter z defines the thickness from the free surface ($z = 0$ mm) to the middle of the specimen ($z = 5$ mm). Then, an unmapped hexahedral dominant mesh was considered for the rest of the model.

The upper crack face was covered by elements CONTA174, while the other one was substituted by elements TARGE170 on the plane symmetry to define the contact during the unloading load steps. The Augmented Lagrangian method with penalty factor 30 and penetration tolerance 0.1 was used in all simulations.

4. Results

4.1. Crack closure evolution

As it was mentioned in chapter 2.2, the crack closure parameter f can be determined in each unloading load step. The evolution of the closure level at the free surface and in the middle of the specimen made of the EA4T steel is shown in Fig. 6. The importance of the LU cycles between the growing cycles and at the end of the simulation can be seen. The parameter f determined during the growing cycles LDU was very different from those obtained in the stabilized phase. It can be seen that there is no crack closure in the middle of the specimen while at the free surface the closure level is around 0.42. Similar trends were obtained also for the rest of materials, see Fig. 7. Shifting of the original stress-strain curve down or a greater hardening leads to a smaller crack closure level. On the other hand, when the bilinear material or the EA4T steel is shifted up, the crack closure parameter increases, see Tab. 1.

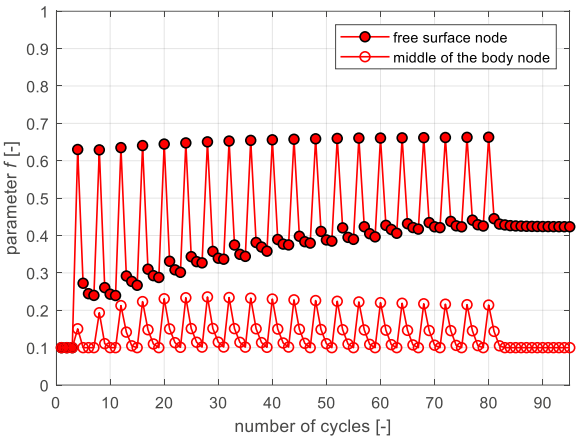

Fig. 6. Closure level evolution – EA4T

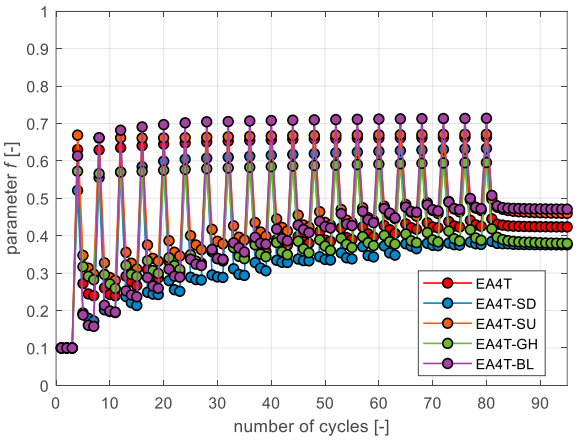

Fig. 7. Closure level at the free surface – all models of materials

Tab. 1. Crack closure levels.

Model of material	EA4T	EA4T-SD	EA4T-UP	EA4T-GH	EA4T-BL
Yield strength σ_y [MPa]	470	310	655	555	420
Element size L_e [mm]	0.0139	0.0319	0.0071	0.0100	0.0174
Element size L_e [mm]	0.0139	0.0319	0.0071	0.0100	0.0174

4.2. Stabilization along the thickness

The crack closure stabilization detail of the depth of 1 mm from the surface of the specimen made of the EA4T steel is shown in Fig. 8. The blue curve ($cyc = 80$) represents results from the last LDU cycle while the rest of the curves were obtained from the following cycles which do not contain the node release. According to the detail of the depth of 1 mm from the free surface, at least five LU cycles are necessary for stabilization of the results and smooth transition. The difference between the result from the first unloading after the last node release (last LDU cycle) and the last cycle of the simulation is shown for all considered materials in Fig. 9.

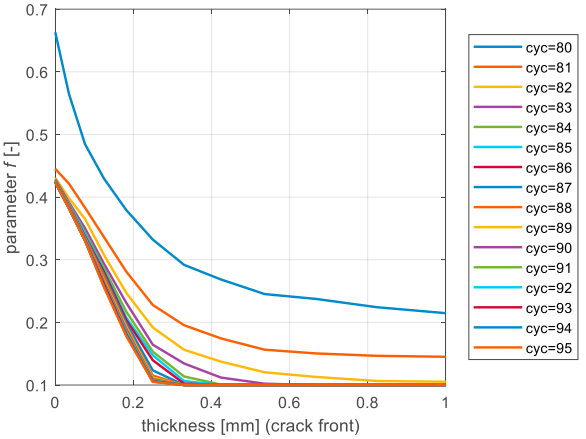

Fig. 8. Closure level saturation detail – EA4T steel

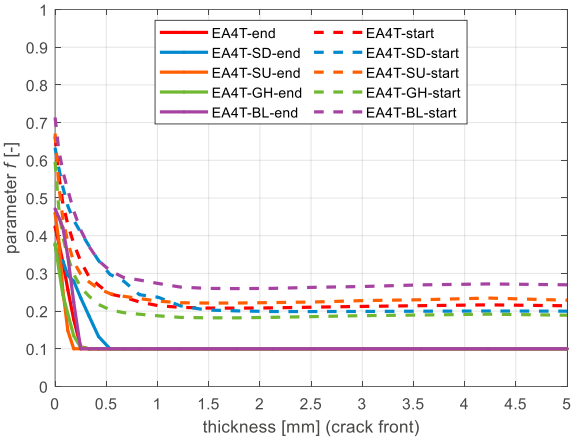

Fig. 9. Closure level through the thickness – all models of materials

Conclusions

The presented work was focused on investigation of different crack closure levels induced by plasticity considering different materials. According to the Newman's estimation the influence of materials characteristics at $R = 0.1$ was negligible, while the experimental results [24] revealed significant differences. The CT specimen with final crack length $a_f = 15$ mm loaded by $K_{max} = 17\ \mathrm{MPa}\sqrt{\mathrm{m}}$ was studied. Different crack closure levels were obtained for different material models using generally adopted assumptions for numerical modelling of PICC. To reach stabilized results, at least five load-unload blocks were necessary to use. The results also showed that crack closure disappears in approximately 80 % of the thickness of the specimen. Therefore, numerical simulations of the crack closure give us promising results to describe differences between plasticity-induced crack closure measured in different materials. However, presented algorithm predicts plasticity-induced crack closure just close to the free surface.

Acknowledgements

This work was financially supported by Czech Science Foundation in frame of the project 22-28283S.

References

[1] W. Elber, Fatigue Crack Closure Under Cyclic Tension, Engineering Fracture Mechanics. 2 (1970) 37–45. https://doi.org/10.1016/0013-7944(70)90028-7.
[2] S. Suresh, Fatigue of Materials, 2nd ed., Cambridge University Press, 1998.
[3] A.K. Vasudeven, K. Sadananda, N. Louat, A review of crack closure, fatigue crack threshold and related phenomena, Materials Science and Engineering A. 188 (1994) 1–22. https://doi.org/10.1016/0921-5093(94)90351-4.
[4] S. Suresh, G.F. Zamiski, D.R.O. Ritchie, Oxide-Induced Crack Closure: An Explanation for Near-Threshold Corrosion Fatigue Crack Growth Behavior, Metallurgical Transactions A. 12 (1981) 1435–1443. https://doi.org/10.1007/BF02643688.
[5] S. Suresh, R.O. Ritchie, A geometric model for fatigue crack closure induced by fracture surface roughness, Metallurgical Transactions A. 13 (1982) 1627–1631. https://doi.org/10.1007/BF02644803.
[6] P. Pokorný, T. Vojtek, L. Náhlík, P. Hutař, Crack closure in near-threshold fatigue crack propagation in railway axle steel EA4T, Engineering Fracture Mechanics. 185 (2017) 2–19. https://doi.org/10.1016/j.engfracmech.2017.02.013.
[7] K. Tazoe, H. Tanaka, M. Oka, G. Yagawa, Near-threshold fatigue crack propagation without oxide-induced crack closure, Scientific Reports 2020 10:1. 10 (2020) 1–8. https://doi.org/10.1038/s41598-020-64915-3.
[8] N.A. Fleck, Finite Element Analysis of Plasticity-Induced Under Plane Strain Conditions, Eng Fract Mech. 25 (1986).
[9] A.F. Blom, D.K. Holm, An Experimental and Numerical Study of Crack Closure, Engineering Fracture Mechanics. 22 (1985) 997–1011.

[10] J.C. Jr. Newman, A Finite-Element analysis of fatigue crack closure, Mechanics of Crack Growth, ASTM STP 590. (1976) 281–301.
[11] M. Nakagaki, S.N. Atluri, An elastic-plastic analysis of fatigue crack closure in modes I and II, AIAA. 18 (1980) 1110–1117. https://doi.org/doi:10.2514/6.1979-758.
[12] J.D. Dougherty, T.S. Srivatsan, J. Padovan, Fatigue crack propagation and closure behavior of modified 1070 steel: Finite element Study, Engineering Fracture Mechanics. 56 (1997) 167–187. https://doi.org/10.1016/S0013-7944(96)00103-8.
[13] D. Camas, J. Garcia-Manrique, B. Moreno, A. Gonzalez-Herrera, Numerical modelling of three-dimensional fatigue crack closure: Mesh refinement, International Journal of Fatigue. 113 (2018) 193–203. https://doi.org/10.1016/J.IJFATIGUE.2018.03.035.
[14] D. Camas, J. Garcia-Manrique, F. v. Antunes, A. Gonzalez-Herrera, Three-dimensional fatigue crack closure numerical modelling: Crack growth scheme, Theoretical and Applied Fracture Mechanics. 108 (2020) 102623. https://doi.org/10.1016/J.TAFMEC.2020.102623.
[15] D. Camas, J. Garcia-Manrique, F. Perez-Garcia, A. Gonzalez-Herrera, Numerical modelling of three-dimensional fatigue crack closure: Plastic wake simulation, International Journal of Fatigue. 131 (2020) 105344. https://doi.org/10.1016/J.IJFATIGUE.2019.105344.
[16] P. Lopez-Crespo, D. Camas, A. González-Herrera, J.R. Yates, E.A. Patterson, J. Zapatero, Numerical and Experimental Analysis of Crack Closure, Key Engineering Materials. 385–387 (2008) 369–372. https://doi.org/10.4028/www.scientific.net/KEM.385-387.369.
[17] P. Hutař, L. Náhlík, Z. Knésl, Quantification of the influence of vertex singularities on fatigue crack behavior, Computational Materials Science. 45 (2009) 653–657. https://doi.org/10.1016/j.commatsci.2008.08.009.
[18] P. Hutař, L. Náhlík, Z. Knésl, The effect of a free surface on fatigue crack behaviour, International Journal of Fatigue. 32 (2010) 1265–1269. https://doi.org/10.1016/j.ijfatigue.2010.01.009.
[19] J.P.P. Benthem, State of stress at the vertex of a quarter-infinite crack in a half-space, International Journal of Solids and Structures. 13 (1977) 479–492. https://doi.org/10.1016/0020-7683(77)90042-7.
[20] L.P. Pook, Some implications of corner point singularities, Engineering Fracture Mechanics. 48 (1994) 367–378. https://doi.org/10.1016/0013-7944(94)90127-9.
[21] NASGRO 4.0 - Reference Manual, Fracture Mechanics and Fatigue Crack Growth Analysis Software. (2002) 112. https://doi.org/10.1016/s1369-7021(03)00949-0.
[22] J.C.Jr. Newman, A Crack-Closure Model for Predicting Fatigue Crack Growth under Aircraft Spectrum Loading, Methods and Models for Predicting Fatigue Crack Growth Under Random Loading. (1981) 32–53. https://doi.org/10.1520/STP28334S.
[23] D.S. Dugdale, Yielding of steel sheets containing slits, Journal of the Mechanics and Physics of Solids. 8 (1960) 100–104. https://doi.org/10.1016/0022-5096(60)90013-2.
[24] T. Vojtek, P. Pokorný, T. Oplt, M. Jambor, L. Náhlík, D. Herrero, P. Hutař, Classically determined effective ΔK fails to quantify crack growth rates, Theoretical and Applied Fracture Mechanics. 108 (2020). https://doi.org/10.1016/j.tafmec.2020.102608.
[25] ASTM E647, Standard Test Method for Measurement of Fatigue Crack Growth Rates, ASTM International, 2015. https://doi.org/10.1520/E0647-15E01.
[26] N.A. Fleck, Compliance methods for measurement of crack length, in: K.J. Marsh, R. a: Smith, R.O. Ritchie (Eds.), Fatigue Crack Measurement: Techniques and Applications, Engineering Materials Advisory Services Ltd, West Midlands, 1991: pp. 69–93.
[27] J.M. Vasco-Olmo, F.A. Díaz, A. García-Collado, R. Dorado-Vicente, Experimental evaluation of crack shielding during fatigue crack growth using digital image correlation, Fatigue & Fracture of Engineering Materials & Structures. 38 (2015) 223–237. https://doi.org/10.1111/FFE.12136.
[28] P. Lopez-Crespo, A. Steuwer, T. Buslaps, Y.H. Tai, A. Lopez-Moreno, J.R. Yates, P.J. Withers, Measuring overload effects during fatigue crack growth in bainitic steel by synchrotron X-ray diffraction, International Journal of Fatigue. 71 (2015) 11–16. https://doi.org/10.1016/J.IJFATIGUE.2014.03.015.
[29] S.J. Park, Y.Y. Earmme, J.H. Song, Determination of the Most Appropriate Mesh Size for a 2-D Finite Element Analysis of Fatigue Crack Closure Behaviour, Fatigue & Fracture of Engineering Materials & Structures. 20 (1997) 533–545. https://doi.org/10.1111/j.1460-2695.1997.tb00285.x.
[30] K. Solanki, S.R. Daniewicz, J.C.Jr. Newman, Finite element modeling of plasticity-induced crack closure with emphasis on geometry and mesh refinement effects, Engineering Fracture Mechanics. 70 (2003) 1475–1489. https://doi.org/10.1016/S0013-7944(02)00168-6.
[31] F. v Antunes, L.F.P. Borrego, J.D. Costa, J.M. Ferreira, A numerical study of fatigue crack closure induced by plasticity, Fatigue & Fracture of Engineering Materials & Structures. 27 (2004) 825–835. https://doi.org/10.1111/j.1460-2695.2004.00738.x.
[32] R.C. McClung, H. Sehitoglu, On the finite element analysis of fatigue crack closure-1. Basic modeling issues, Engineering Fracture Mechanics. 33 (1989) 237–252. https://doi.org/10.1016/0013-7944(89)90027-1.
[33] C. Gardin, S. Fiordalisi, C. Sarrazin-Baudoux, M. Gueguen, J. Petit, Numerical prediction of crack front shape during fatigue propagation considering plasticity-induced crack closure, International Journal of Fatigue. 88 (2016) 68–77. https://doi.org/10.1016/j.ijfatigue.2016.03.018.
[34] J.C. Newman Jr, FASTRAN-2: A fatigue crack growth structural analysis program, NASA STI/Recon Technical Report N. 92 (1992) 30964.
[35] J.C.Jr. Newman, A crack opening stress equation for fatigue crack growth, International Journal of Fracture. 24 (1984) 131–135.
[36] K. Solanki, S.R. Daniewicz, J.C. Jr. Newman, Finite element analysis of plasticity-induced fatigue crack closure: An overview, Engineering Fracture Mechanics. 71 (2004) 149–171. https://doi.org/10.1016/S0013-7944(03)00099-7.
[37] K.D. Singh, M.R. Parry, I. Sinclair, Some issues on finite element modelling of plasticity induced crack closure due to constant amplitude loading, International Journal of Fatigue. 30 (2008) 1898–1920. https://doi.org/10.1016/j.ijfatigue.2008.01.013.
[38] N.A. Fleck, J.C. Jr. Newman, Analysis of crack closure under plane strain conditions, Mechanics of Fatigue Crack Closure. (1988) 319–341.